Fluorescence Lifetime Imaging of Mixing Dynamics in Continuous-Flow Microdroplet Reactors

Monpichar Srisa-Art,[1] Andrew J. deMello,[1,*] and Joshua B. Edel[1,2,*]

[1]*Department of Chemistry, Imperial College London, South Kensington, London SW7 2AZ, United Kingdom*
[2]*Institute of Biomedical Engineering, Imperial College London, South Kensington, London SW7 2AZ, United Kingdom*

(Received 3 February 2008; published 2 July 2008)

Water-in-oil microdroplets within fluidic channels have the potential to serve as isolated reaction compartments for monitoring real-time dynamics with high efficiency and repeatability. Droplets, usually generated from aqueous and oil solutions using standard microfluidic formats, can be produced at frequencies in excess of 1 kHz. Although mixing within such microdroplets is normally enhanced by chaotic advection, the mixing pattern from droplet to droplet is almost identical and reproducible in form. Herein, we demonstrate that fluorescence lifetime imaging can be used to reconstruct mixing patterns within a droplet with a time resolution of 5 μs.

DOI: 10.1103/PhysRevLett.101.014502 PACS numbers: 47.61.Ne, 83.50.Xa

In recent years, microfluidic systems have matured into efficient instrumental formats for performing high-throughput chemistry and biology [1,2]. Of particular current interest are microfluidic systems which make use of flow instabilities between immiscible fluids to generate suspended droplets [1]. Put simply, droplets can be made to spontaneously form when laminar streams of aqueous reagents are injected into an immiscible carrier fluid. Droplets are typically generated in continuous-flow systems using either the T-junction or flow-focusing methods [3–8]. In the former, the continuous and disperse phases are injected from orthogonal branches of a microfluidic tee-junction. Droplets (the disperse phase) occur as a result of shear forces and interfacial tension at the fluid-fluid interface. In the latter, the continuous phase is introduced via two flanking channels with the disperse phase being injected through a central channel into a narrow orifice.

In conventional (single-phase) microfluidic systems, fluid properties are predominantly controlled by viscous rather than inertial forces, and flow is essentially laminar [2]. This behavior has a significant consequence on mixing. In its simplest manifestation, mixing occurs by uniting pure fluid-component streams. Since the only route to mixing is via diffusion across fluidic interfaces (due to the absence of fast convective processes that dominate in turbulent systems), mixing times can be long, and residence time distributions appreciable [9]. Accordingly, there have been numerous reports describing new approaches to enhance microfluidic mixing [10–13]. Of particular note is the use of twisting channel geometries to generate chaotic mixing within droplets by folding, stretching, and reorienting fluid elements. Consequently, mixing within droplets is rapid, and reagent transport occurs with no dispersion. This innovation has enabled droplet-based microfluidic systems to overcome the problems of slow mixing and dispersion [14–16]. Indeed, recently droplet-based microfluidic systems have been used to monitor reactions on the millisecond time scale [8,17]. In this Letter, we build on these developments and show that fluorescence lifetime imaging (FLIM) can be used to monitor mixing with a temporal resolution of approximately 5 microseconds. Specifically, FLIM can be used to reconstruct mixing patterns within a droplet with a time resolution of 5 μs or 20 photons. A maximum likelihood estimator approach, adapted from single molecule fluorescence lifetime studies, allows us to determine the fluorescence lifetime and build up of the two-dimensional map of droplet mixing.

In the current microdroplet system, a 10:1 (v/v) mixture of perfluorodecalin and 1H, 1H, 2H, 2H-perfluorooctanol and aqueous solutions was continuously pumped through a T-junction microfluidic device (Fig. 1) at a constant volumetric flow rate of 1.5 μl min^{-1}, resulting in the total volumetric flow rate of 3.0 μl min^{-1} (and linear fluid velocity of 20.0 mm s^{-1}). The first aqueous inlet consisted of a 20 μM fluorescein 5-isothiocyanate (FITC) solution (in pH 9.0 buffer) delivered at a flow rate of 0.75 μl min^{-1}. A 10 μM rhodamine 110 chloride (Rh 110) solution (in pH 9.0 buffer) was pumped into the second aqueous inlet at a flow rate of 0.75 μl min^{-1}. Fluorescence lifetimes were recorded at the first loop of the winding channel, which is 259.7 μm (or ~13 ms) downstream of the droplet forming region, and then moved along the winding part. The detection probe volume was positioned at half the depth of the main channel (25 μm) in the vertical dimension, and scanned (in 1 dimension) at 1 μm intervals

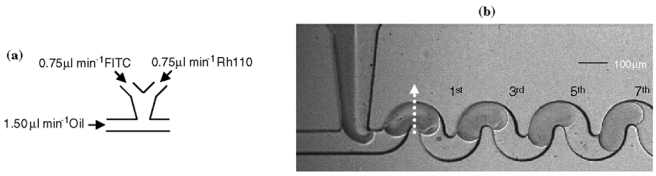

FIG. 1 (color online). (a) Schematic of the microfluidic device. The 50 μm square cross section microchannel network consists of 3 inlets and 1 outlet. (b) An example image of droplets generated. An arrow shows the scanning direction.

across the 50 μm wide channel to allow reconstruction of the mixing pattern for a single droplet. Fluorescein 5-isothiocyanate and rhodamine 110 chloride, were used for droplet-lifetime measurements, since they possess significantly different lifetimes (FITC has a lifetime of 4.1 ns at pH 9 while Rh 110 has a lifetime of 2.9 ns at the same pH).

Fluorescence was recorded with a time-resolved scanning confocal spectrometer. A 438 nm picosecond laser operating at a repetition rate of 20 MHz is used to excite analyte molecules within the detection probe volume. When a photon is registered, the time correlated single photon counting (TCSPC) electronics designate its arrival time relative to the first excitation pulse. Therefore, each photon is assigned its arrival time, $t_1, t_2, \ldots, t_n$. The photons themselves are recorded with 28 ps resolution with respect to the laser pulse. These arrival times are then rebinned to extract fluorescence lifetime and intensity information. The molecular fluorescence lifetime is extracted from the measured fluorescence lifetime by deconvoluting the instrument response function. In the current studies, a solution of Auramine-O was used to determine the instrument response function as it has a lifetime of a few picoseconds [18]. When extracting fluorescence lifetimes from experimentally measured decays containing in excess of 2000 photon counts, a least squares (LS) approach is conventionally used [19]. However, when extracting fluorescent lifetimes from decays containing between 10 and 2000 counts, alternative mechanisms are needed.

One of the most powerful approaches to this problem is via the use of the maximum likelihood estimator (MLE) method [20–22]. With high photon counts, a LS approach can be used to calculate the fluorescence lifetime as it is represented by Gaussian statistics (i.e., as the number of photons increase, the measured lifetime goes from Poissonian and multinomial statistics and converges to Gaussian statistics). However, when determining a fluorescence lifetime with few photons, an MLE and not an LS is more appropriate as this is defined by multinomial statistics.

The MLE (γ_i) is defined by Eq. (1),

$$\gamma_j = \sum_{1}^{k} n_i \log\left(\frac{n_i}{N p_i(j)}\right). \tag{1}$$

Here, n_i is the number of photon counts in channel i, i is the summation index, starting at 1, k is the number of channels (or bins) for each fluorescence decay, and $p_i(j)$ is the probability that a group of photons will fall in channel i if the particles have a lifetime j [23]. $N = \Sigma_1^k n_i$ is the total number of counts for a given decay. In simple terms, the MLE approach essentially determines the occurrence probability of a specific lifetime.

Although there have been many attempts to develop simple and elegant solutions to Eq. (1), Edel *et al.* [24] recently demonstrated that for a monoexponential decay, the MLE convolved with an instrument response function (IRF) can be given by Eq. (2). This approach relies on minimizing a function that contains both the fluorescence decay as well as an IRF contribution. Using this algorithm, as little as 20 photons can be used to accurately determine a fluorescence lifetime [24].

$$\frac{N}{1 - e^{-\omega/r}} - \frac{Nk}{e^{k\omega/\tau} - 1} = \sum_{i=1}^{k} i n_i \left(\frac{i - \sum_{j=1}^{i} j r_j e^{j\omega/\tau}}{\sum_{j=1}^{i} r_j e^{j\omega/\tau}}\right). \tag{2}$$

The IRF contribution to the decay corresponds to r_j in each bin j recorded with a time resolution ω. The fluorescence lifetime, τ, can then be determined by solving for the local minimum. Importantly, there is a compromise between time resolution and error. For example, fewer recorded photons correlate to a lower temporal resolution (e.g., $N = 20$ correlates to a time resolution of 5 μs while $N = 500$ corresponds to a time resolution of 150 μs).

An example of a time-integrated photon scan is shown in Fig. 2(a). These trajectories were obtained by locating the detection probe volume at a position 25 μm from the channel bed and 10 μm from the channel edge. Each peak represents an aqueous droplet transiting the 350 nm wide diffraction limited detection probe volume. Figure 2(b) illustrates the corresponding fluorescence lifetime temporal variation determined using a customized maximum likelihood estimator algorithm. Each point represents an extracted fluorescence lifetime measured with a maximum of 20 photons. Using our acquisition electronics, this corresponds to an acquisition time of 5 μs per point. In turn, this corresponds to approximately 600 points per droplet in the direction of flow. Comparison of Figs. 2(a) and 2(b) highlights a clear difference in the total number of data points recorded, with the lifetime data having a time resolution approximately 2 orders of magnitude higher than the intensity data. Despite this difference, a close correspondence is seen in the respective trajectories between individual droplets.

It is important to note that the recorded fluorescence intensity is directly proportional to the level of binning. For

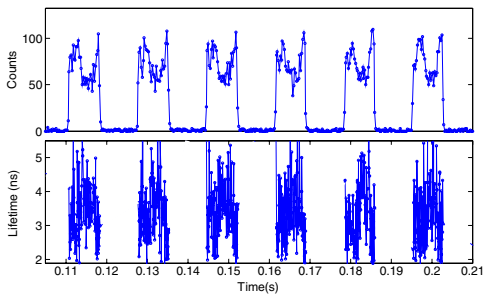

FIG. 2 (color online). An example of plotting a droplet signal intensity trajectory (a) and the fluorescence lifetime determined using a customized maximum likelihood estimator algorithm (b) as a function of time.

example, a signal of 100 photons with a bin time of 1 ms will only have a signal of 10 photons at a bin time of 100 μs. This effect not only modifies the signal-to-noise ratio but also minimizes the possibility of measuring submillisecond traces. A fluorescence lifetime measurement, on the other hand, is intensity independent. Because of the reproducibility of fluidic mixing within a formed droplet, it is possible to maintain high time resolution simply by averaging lifetime data from multiple droplet-lifetime trajectories. The lifetime trajectory of a single droplet can be defined by $[t_1, \ldots, t_p]$, and hence the averaged droplet trajectory can be defined by

$$\bar{\tau} = \frac{1}{p} \sum_{i=1}^{p} \tau_i. \tag{3}$$

With the algorithms used in the current study, a lower limit of 20 photons is necessary for an acceptable fit [24]. Indeed, the error at a single point using 20 photons is 44% measured at a 95% confidence interval. Measuring at the same point within successive droplets brings this error down by the square of the number of droplets sampled. For example, measuring the lifetime over 100 droplets (approximately 1 s of acquisition time) brings the error down to 4.4% while maintaining the same high timing resolution. Similarly, measurement of the same lifetime over 10 000 droplets or 100 s reduces the error to 0.44%. This trend in the reduction of errors is illustrated in Figs. 3(a)–3(e).

Figure 4 shows an example of an interdroplet trajectory taken by averaging 600 droplets. When comparing the lifetime trajectory [Fig. 4(a)] with that of an intensity-based trajectory binned at 10 μs intervals [Fig. 4(b)], several interesting observations can be made. First, a peak in the fluorescence lifetime at approximately 4–5 ms correlates with the fluorescence lifetime of pure FITC. The decrease in the fluorescence signal is directly related to the formation of a multicomponent mixture of both FITC and Rh 110. Consequently, as the overall lifetime decreases, a greater degree of Rh 110 is incorporated in the system. In the intensity-based trajectory, a decrease in signal indicates a greater FITC concentration. As expected, the measured intensity is dependent on the concentration, quantum yield, and absorption cross section of the component dyes. Second, at the droplet boundaries, the time-integrated signal tends towards zero counts. Conversely, in the time-resolved data, the fluorescence lifetime trajectory tends to 2.9 ns (the fluorescence lifetime of pure Rh 110). This discrepancy highlights the fact that analysis of only the time-integrated intensity signal will result in an inaccurate representation of the analytical content within a droplet.

In order to create a two-dimensional representation of mixing within the droplets, lifetime measurements were recorded at different points along the winding microchannel. Fluorescence lifetime data were acquired by precisely scanning the detection probe volume (positioned 25.0 μm from the channel bed) in one-dimension across the 50.0 μm wide channel at 1.0 μm intervals. Photons arrival times were recorded for 20 s at each detection point along the scan direction. Therefore, at the flow conditions used, approximately 600 droplets were recorded over this time period. The fluorescence lifetime trajectories obtained at 50 detection points along the scan direction were then used to build up the 2D image. Figure 5 presents two-dimensional images of a droplet passing through the 1st (a & b), and 3rd (c & d), loop of the winding microchannel. Droplet images were reconstructed either based on fluorescence lifetime [Figs. 5(a) and 5(c)] or fluorescence intensity [Figs. 5(b) and 5(d)] data. Because of the lifetime difference between FITC and Rh 110, intradroplet mixing patterns can be reconstructed from the FLIM data in a facile manner. The y axis in Fig. 5 is defined as the width of the microchannel and width of the microdroplet, while the x axis is the length of the microdroplet. As can be seen in Fig. 5(a), the fluorescence lifetime map at the first loop (13 ms after droplet formation) indicates two emitting components within the droplet, which are incompletely

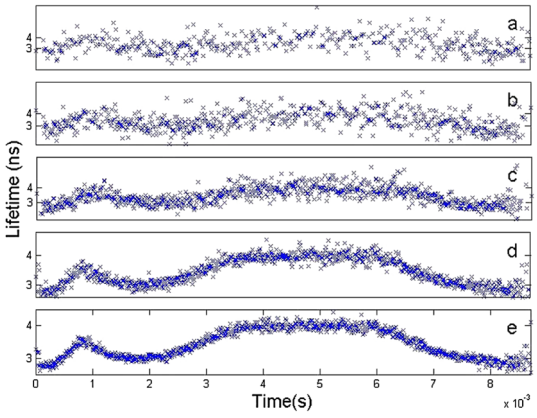

FIG. 3 (color online). High resolution lifetime trajectories. The lifetime data were extracted using (a) 5, (b) 10, (c) 50, (d) 250, and (e) 600 droplets at a single detection point. These trajectories show the reproducible mixing pattern within the droplets.

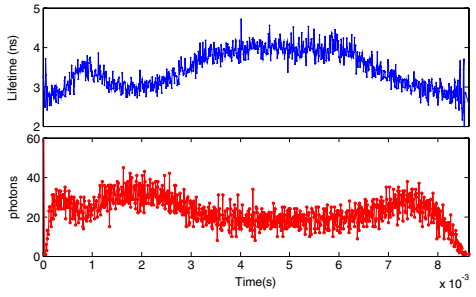

FIG. 4 (color online). Intradroplet trajectories reconstructed by averaging fluorescence data from 600 droplets; (a) lifetime trajectory and (b) intensity-based trajectory binned at 10 μs intervals.

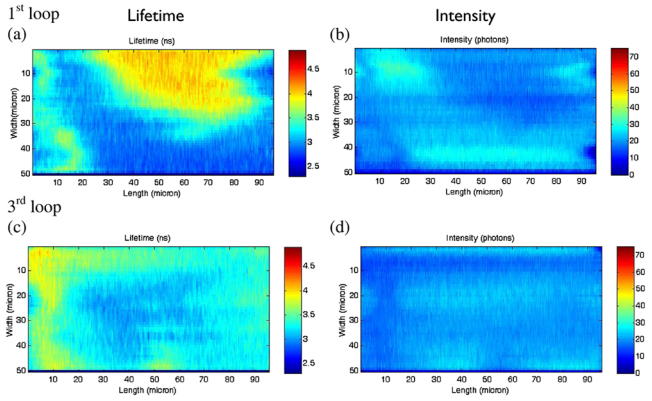

FIG. 5 (color online). Two-dimensional fluorescence maps of reconstructed droplets based on fluorescence lifetime (a) and (c) and fluorescence intensity (b) and (d) at the 1st (a) and (b) and 3rd (c) and (d) loops. The Y axis is the width of the droplet with 0 and 50 μm being the droplet and channel boundary. The X axis represents the length of the droplet with 47 μm being the central point. The images are built up by obtaining trajectories, as shown in Fig. 4, at 50 detection points along the width of the channel.

mixed. The higher fluorescence lifetime of ~4.1 ns towards the upper portion of the droplet represents FITC, whereas the lower lifetime of ~2.9 ns (predominantly towards the lower portion of the droplet) belongs to Rh 110. An intermediate average fluorescence lifetime is found around the middle of the droplet, expressing partial mixing of the two dyes. Similarly, the fluorescence intensity pattern inside a droplet [Fig. 5(b)] also depicts incomplete mixing between FITC and Rh 110. However, in this case, mapping is clearly affected by a reduced signal-to-noise ratio and intensity fluctuations not associated with the mixing dynamics. Improved mixing is observed in Figs. 5(c) and 5(d) at the 3rd loop. An average fluorescence lifetime (between that of pure FITC and Rh 110) of ~3.5 ns occurs in most areas of the droplet [Fig. 5(c)]. However, a lifetime of ~4.0 ns belonging to FITC is found at the back of the droplet (on the left of the image) rather than towards the top.

In conclusion, we have shown that fluorescence lifetime imaging can be used to successfully reconstruct mixing patterns inside picoliter volume droplets with a temporal resolution of 5 μs; this is several orders of magnitude lower than what has previously been reported. We expect that the ability to monitor mixing dynamics with such high temporal and spatial resolution will prove to be valuable for facilitating high-throughput, protein-folding studies and chemical reactions with submicrosecond timing resolution.

M. S-A. acknowledges the Royal Thai Government for financial support. The work was partially supported by the RCUK funded Microdroplets Basic Technology Project.

*a.demello@imperial.ac.uk, joshua.edel@imperial.ac.uk

[1] H. Song, D. L. Chen, and R. F. Ismagilov, Angew. Chem., Int. Ed. Engl. **45**, 7336 (2006).
[2] A. J. deMello, Nature (London) **442**, 394 (2006).
[3] P. Garstecki, M. J. Fuerstman, H. A. Stone, and G. M. Whitesides, Lab Chip **6**, 437 (2006).
[4] J. H. Xu, S. W. Li, J. Tan, Y. J. Wang, and G. S. Luo, AIChE J. **52**, 3005 (2006).
[5] P. Garstecki, I. Gitlin, W. DiLuzio, G. M. Whitesides, E. Kumacheva, and H. A. Stone, Appl. Phys. Lett. **85**, 2649 (2004).
[6] M. M. Dupin, I. Halliday, and C. M. Care, Phys. Rev. E **73**, 055701 (2006).
[7] A. Huebner, M. Srisa-Art, D. Holt, C. Abell, F. Hollfelder, A. J. deMello, and J. B. Edel, Chem. Commun. (Cambridge) 12 (2007) 1218.
[8] M. Srisa-Art, A. J. deMello, and J. B. Edel, Anal. Chem. **79**, 6682 (2007).
[9] S. Krishnadasan, R. J. C. Brown, A. J. Demello, and J. C. Demello, Lab Chip **7**, 1434 (2007).
[10] F. G. Bessoth, A. J. deMello, and A. Manz, Anal. Commun. **36**, 213 (1999).
[11] M. Heule and A. Manz, Lab Chip **4**, 506 (2004).
[12] B. Zheng, C. J. Gerdts, and R. F. Ismagilov, Curr. Opin. Struct. Biol. **15**, 548 (2005).
[13] M. R. Bringer, C. J. Gerdts, H. Song, J. D. Tice, and R. F. Ismagilov, Phil. Trans. R. Soc. A **362**, 1087 (2004).
[14] H. Song, J. D. Tice, and R. F. Ismagilov, Angew. Chem., Int. Ed. Engl. **42**, 768 (2003).
[15] D. R. Link, E. Grasland-Mongrain, A. Duri, F. Sarrazin, Z. Cheng, G. Cristobal, M. Marquez, and D. A. Weitz, Angew. Chem., Int. Ed. Engl. **45**, 2556 (2006).
[16] A. D. Griffiths and D. S. Tawfik, Trends Biotechnol. **24**, 395 (2006).
[17] H. Song and R. F. Ismagilov, J. Am. Chem. Soc. **125**, 14613 (2003).
[18] J. B. Edel and A. J. Demello, Appl. Phys. Lett. **90**, 053904 (2007).
[19] M. J. van der Meer, H. Zhang, and M. Glasbeek, J. Chem. Phys. **112**, 2878 (2000).
[20] M. Maus, M. Cotlet, J. Hofkens, T. Gensch, F. C. De Schryver, J. Schaffer, and C. A. M. Seidel, Anal. Chem. **73**, 2078 (2001).
[21] M. Kollner, A. Fischer, J. ArdenJacob, K. H. Drexhage, R. Muller, S. Seeger, and J. Wolfrum, Chem. Phys. Lett. **250**, 355 (1996).
[22] P. Hall and B. J. Selinger, J. Phys. Chem. **85**, 2941 (1981).
[23] M. Kollner and J. Wolfrum, Chem. Phys. Lett. **200**, 199 (1992).
[24] J. B. Edel, J. S. Eid, and A. Meller, J. Phys. Chem. B **111**, 2986 (2007).